Progress In Electromagnetics Research C, Vol. 135, 157–172, 2023

Intelligent Sensor System with Transmission Coefficient in X-Band Frequency for Determining Sugar Content

Pornpimon Chaisaeng[1], Thunyawat Limpiti[2], and Prapan Leekul[1, *]

Abstract—This study describes a non-contact low-cost X-band sensor system for determining the soluble solid content (SSC) of a sugar solution. The system adopts a transmission signal technique with two frequency pairs (10.2 GHz paired with 10.4 GHz and 10.2 GHz paired with 10.6 GHz) from three transceiver modules. Each module has a microstrip patch antenna, mixer circuit, and dielectric resonator oscillator. To simplify the transmission power frequency of each frequency pair, the frequency is down-converted to an intermediate frequency (IF) signal using a frequency mixer. The IF signals are then compared using a gain and phase detector to find their magnitude ratio and phase difference. The measured SSC-level data are randomly divided into three datasets and input to an artificial neural network (ANN) for training. The training output is the SSC level in Brix degree. The proposed ANN structure comprises four input nodes, eight hidden nodes, and four output nodes, affording low complexity and resource savings while providing 92.98% accuracy. Therefore, the proposed low-cost sensor system can achieve precise decision-making and real-time measurement.

1. INTRODUCTION

Sugar provides the energy required for organ function in the human body, but excessive sugar consumption affects our health and can cause various diseases [1], thus sugar consumption control is important. Excess sugar consumption causes serious complications in diabetes patients [2], with a global estimate of 425 million for adults in 2017 [3]. The World Health Organization (WHO) recommends that adults limit sugar intake to no more than 5% of their total energy intake from food and beverages per day [4], but avoiding sugar intake is impossible because human food contains some sugar in natural foods and as raw materials for production or food preservatives [5]. Several countries have enacted food taxes [6] and must show the amount of sugar on food product labels for the good health of the population; however, various foods cannot show the amount of sugar, thus sugar content measurement in food is important [7]. A high accuracy sugar content measurement method for liquid food was liquid chromatography, which separates a sample into its chemical composition [8]. This technique is limited to its application in the food manufacturing process because it is a contact and destructive method, non-real-time processing, sample preparation before measurement, time-consuming, and expensive. Refractometers were commonly used to measure sugar content in beverages [9], fruit juice [10], or wine processing [11, 12]. This technique was based on measuring the refractive index of sugar solution in realtime and at a low cost; however, it was a contact method. Therefore, this study presented several non-contact and real-time sugar measurement techniques. The sugar content measurement technique with near infrared (NIR) spectroscopy based on absorption or emission at NIR range was presented with a high accuracy method [13–16], but its application in the process was limited because it required a

Received 4 April 2023, Accepted 13 July 2023, Scheduled 30 July 2023

* Corresponding author: Prapan Leekul (prapan.l@rbru.ac.th).

[1] Department of Electrical Engineering, Faculty of Industrial Technology, Rambhai Barni Rajabhat University, Chanthaburi 22000, Thailand. [2] Department of Electrical Engineering, School of Engineering and Technology, Walailak University, Nakhon Si Thammarat 80160, Thailand.

computer for a lot of data processing. A suitable environment, light condition, and temperature control were necessary for field measurements. These factors strongly affect the system measurement, mostly the NIR system experiment, which is still a laboratory test. The sugar content measurement with a light source and a prism based on the refractive index of sugar solution [17] was less expensive, but still limited in its application in real-world processes. Microwave is an intriguing technique for measuring sugar content, and it is commonly used in industry because of its nondestructive and realtime processing [18]. Microwave sugar content measurement is based on the dielectric properties of sugar solution, which differs at each sugar content level [19]. Sugar content determination techniques from a sensitivity of radio frequency identification (RFID) tag antenna operating frequency range of 860–960 MHz [20] and from a shifted resonance frequency of the resonator [21] are examples of effects on microwave propagation characteristics. Both methods were non-contact, and their RFID and resonators were low profile and low cost, but they required an expensive measurement device, making them unsuitable for real applications. The reflection coefficient of the microstrip antenna was another method for determining the sugar content that was laid on the sugar solution [22–24]. This method has low complexity and microwave power measurement, which can be developed for real application with a low-cost circuit. Furthermore, the transmission coefficient is related to the sugar content of sugar solution [25], allowing for developing sugar content determination in sugar solution systems based on transmission signals, allowing for non-contact and non-destructive sample measurement. Another important issue for sensor systems is the precision and simplicity of the processor. Artificial neural networks (ANNs) are data analysis algorithms that are widely used in microwave measurement systems because they are suitable for nonlinear systems and high efficiency [26, 27], multiple-input, and complicated interactions between input and output [28]. ANNs are the type of artificial intelligence system that is mathematically modeled after the human neural system and is capable of patterning, language comprehension, perceiving, and responding. Therefore, researchers were eager to use ANNs for data processing and sensor system analysis [29]. Thus, the presented sugar content determination sensor system used a low complexity transmission microwave signal, real-time processing, and ANNs for system processor that can be implemented in microcontrollers, then reduce system costs and suitable for field application.

This study used the transmission of a triple-frequency electromagnetic wave in the X-band to determine the soluble solid content of sugar solution using 2 frequency pairs of 10.2 with 10.4 GHz and 10.2 with 10.6 GHz. The received signal was mixed with local frequency at each paired module and selected low frequency to process for system simplification. The magnitude ratio (V_{MAG}) of the two IF signals (one from each module pair) and their phase difference (V_{PHS}) were calculated as the input data of ANNs training and SSC analysis. Section 2 is dielectric properties measurement of sugar solution with different SSC levels using an open-ended coaxial dielectric probe and then calculating the difference of dielectric constant (ε'_r) and dielectric loss factor using a vector network analyzer (VNA). Section 3 is sugar solution model development based dielectric properties for SSC determination of sensor system simulation then analyzes the capability of soluble solid content classification from the magnitude and phase of transmission signal comparison. Section 4 presents a low-cost X-band sensor system with triple-frequency development by a motion detector module application that was developed and tuned to operate at 10.2, 10.4, and 10.6 GHz, the control of electromagnetic wave transmission, and signal mixing, as well as RF switch control for receiving signals from each module pair to magnitude and phase comparison. Section 5 analyzes the magnitude and phase change of measured IF signal from a sugar solution with SSC levels ranging from 3, 6, 9, to 45° Brix for ANNs training. Section 6 consists of training and testing ANNs with V_{MAG1}, V_{MAG2}, V_{PHS1}, and V_{PHS2}, ANNs structure adaptation and decision capability development of ANNs, ° Brix error analysis at each level, and discussion. Section 7 is the conclusion.

2. DIELECTRIC PROPERTY OF SUGAR SOLUTION

The sugar solution for dielectric properties measurement was natural cane syrup for cooking brought from a local market, which consists of sucrose, glucose, and fructose. The syrup was diluted with water in proper ratio to prepare the sugar solution with SSC of 3 to 45° Brix using YOG339K Brix refractometer to measure the SSC of diluted sugar solution. The dielectric properties of the sugar solution were measured using Keysight N1501A dielectric probe kit, processed with field fox N9916A

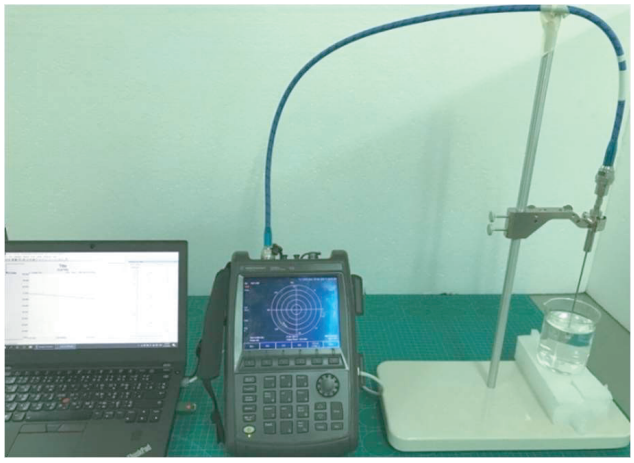

Figure 1. Dielectric property measurement of sugar solution.

VNA and calculated for dielectric properties with program Keysight material measurement suite version 18.0 to display the dielectric constant and dielectric loss factor. The VNA was calibrated with 3 steps before measurement by 1) open with air 2) short circuit with short block, and 3) loaded with 25°C water. The sample sugar solution for the dielectric constant ε_r' and dielectric loss factor ε_r'' measurement volume was 250 ml and contained in a standard beaker (Fig. 1).

The dielectric of sugar solution from [30] showed the SSC effect to the change of ε_r' and ε_r''; at the frequency of 10 GHz, when the SSC is increased, ε_r' decreases linearly, and ε_r'' decreases following the same trend. The change in the dielectric properties affected the transmission signal, reflection signal, and power absorption. Therefore, in this study, the dielectric properties were measured with sugar solution samples consisting of 14 samples from 3, 6, 9, 13 to 45° Brix with three frequencies 10.2, 10.4, and 10.6 GHz. The ε_r' of water was in the range of 61.94 to 62.83, then measured ε_r' of sugar solution with 3° Brix 61.73 to 60.86, and ε_r' linear decreases continuously when SSC increases from 6, 9, 13, 19 to 45° Brix. The measurement result of the ε_r'' of water was in the range of 26.12 to 33.14; the ε_r'' change was clear when SSC increased from 3 to 45° Brix. The measured ε_r' and ε_r'' of the sugar solution are shown in Fig. 2.

The ε_r' and ε_r'' in 3 frequencies decreased as SSC of sugar solution increased, especially ε_r', indicating that SSC of sugar solution significantly affects ε_r' in frequencies 10.2, 10.4, and 10.6 GHz. When SSC of

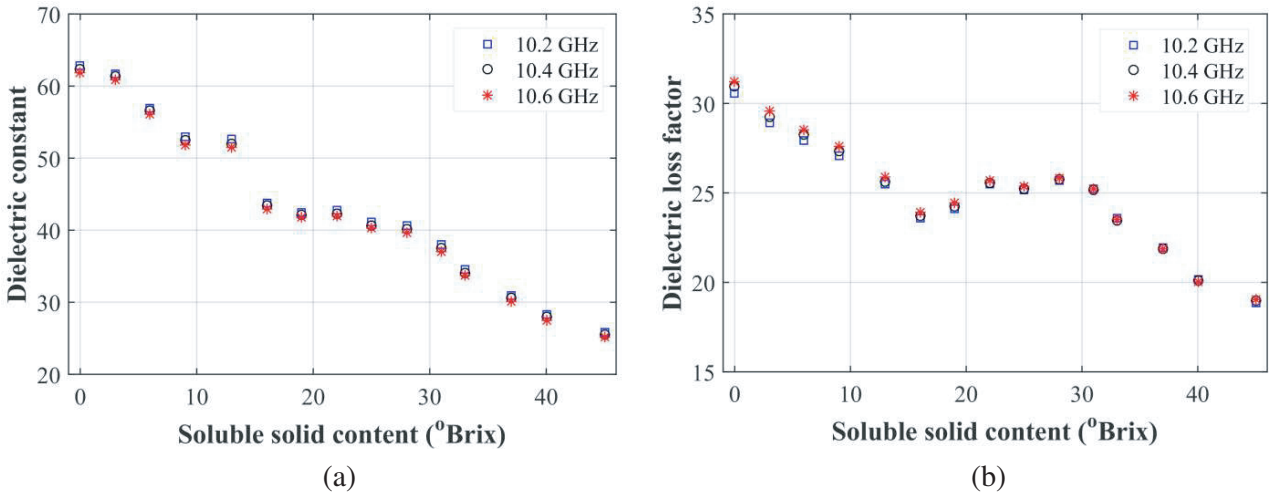

Figure 2. (a) Dielectric constant and (b) dielectric loss factor of sugar solution.

sugar solution increases, the free molecules of water are replaced by solute molecules. As a consequence, the water behavior was decreased [31], thus dielectric constant of solution decreases according to the increase in SSC quantities. The dielectric constant of soluble solids is lower than water, and the dielectric loss factor decreases due to the orientation of the water and solute molecules [32]. This shows the ability to classify SSC of sugar solution using triple-frequency transmission signal analysis. Furthermore, the ε'_r of sugar solution with each SSC was used to model sugar solution sample in sensor system simulation for ability analysis of SSC classification from X-band frequency transmission signal technique.

3. SSC DETERMINATION SIMULATION

The efficiency simulation SSC determination of system analysis in sugar solution by triple X-band frequency transmission technique antenna was simulated for the first time using microstrip patch because the simulation system was structured identically to the system that would actually be built from HB 100 modules which was small and low cost for cost reduction [33, 34]. Therefore, the modeled antenna was designed to operate in wideband with the same properties as the embedded antenna in the HB 100 module. Microstrip antenna has low profile and potential for miniaturization [35], and the dielectric properties of substrate are important in considerations of model antenna design to optimize antenna size, radiation efficiency, and bandwidth [36]. The geometry of the patch antenna was designed using the physical cut-and-try method for operating frequencies ranging from 10.2 to 10.6 GHz using the CST studio suite simulator, which then provided optimized dimension and antenna characteristics. The S_{11} of antenna 1 at frequencies 10.2 10.4, and 10.6 GHz was -18.1, -24.47, and -28.96 dB; that of antenna 2 was -18.37, -25.55, and -29.29 dB; that of antenna 3 was -19.16, -27.28, and -33.76 dB, respectively (Fig. 3).

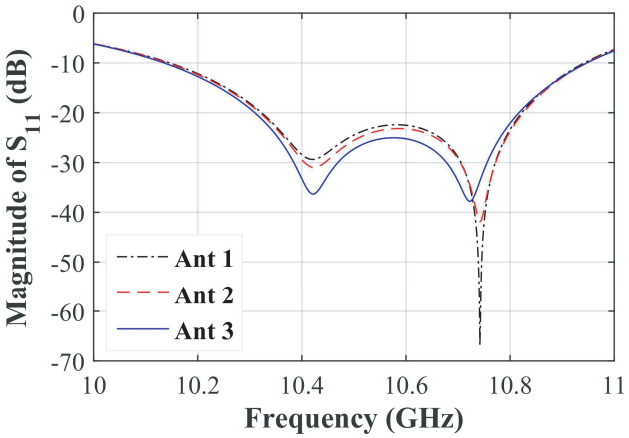

Figure 3. Return loss of antennas.

In sensor system simulation for magnitude and phase of transmission signal analysis, antenna models were used in the simulation for transmitting and receiving signals, in which antenna 1 operated at frequency 10.2 GHz and placed opposite to antenna 2, and antenna 3 operated at frequency 10.4 GHz and 10.6 GHz, respectively. The position of three antennas was in far field region of the lowest frequency 10.2 GHz and reduced the signal coupling between antenna 2 and antenna 3. At the middle of 3 antennas was acrylic sample holder model with size $3.2 \times 7.2 \times 18.2$ cm which contained sugar solution model with ε'_r related to SSC level from 24 to 64, and ε''_r was taken as the average value (25.42) and height 7 cm (Fig. 4(a)). In the sensor system simulation, the shape of radiation pattern of antenna 1 during measuring had changed due to radiation pattern responding to ε_r of sugars solution and sample holder model (Fig. 4(b)). It showed a response of antenna to the measured material.

The transmission signal power was mixed to analyze intermediate frequency (IF) signal by frequency mixer that operates to multiply 2 input signals when input 1 is received signal $V_{Rx}\cos(2\pi f_{Rx}t + \phi)$, and input 2 is local signal $V_{LO}\cos(2\pi f_{LO}t)$. Then output V_{IF} is filtered for using only in low frequency

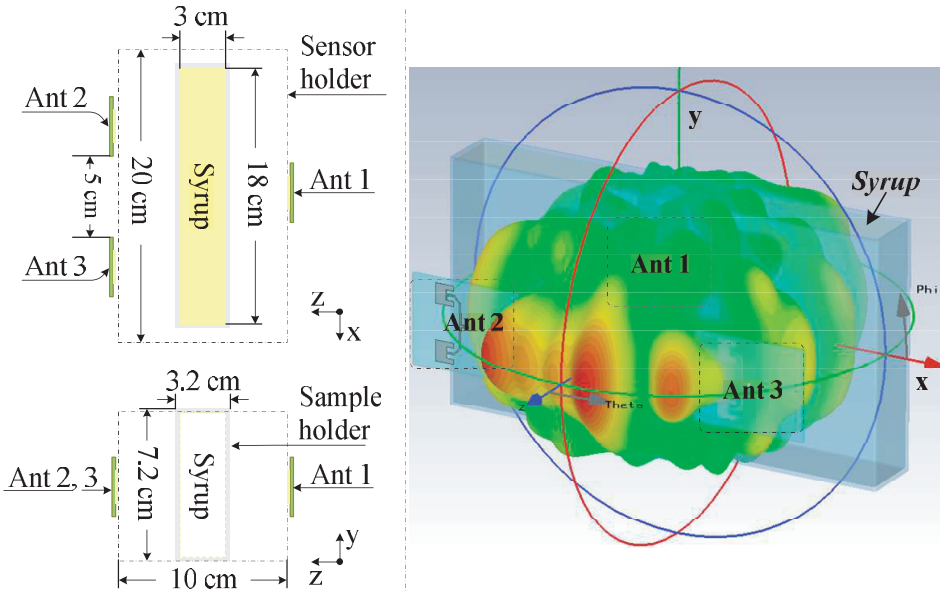

Figure 4. (a) Simulation geometry of SSC determination sensor system and (b) radiation pattern of antenna 1.

that equal to the difference between f_{Rx} and f_{LO} [37] as shown in Equation (1).

$$V_{IF}(t) = \frac{V_{Rx}V_{LO}}{2}\cos\left[2\pi(f_{Rx} - f_{LO})t + \phi\right] \tag{1}$$

The transmission signal power of the first pair, which was $\mathbf{S}_{12}$ and $\mathbf{S}_{21}$, was mixed to analyze V_{IF} consisting of magnitude in dB and phase (ϕV_{IF}) in degree by mixer equation, where local oscillator (LO) signal at each receiver had 0 dB magnitude and 0° degree phase. The transmission signal power of the second pair was $\mathbf{S}_{13}$ and $\mathbf{S}_{31}$ which were also analyzed by Equations (2)–(3)

$$V_{IF}\,(\text{dB}) = V_{LO}\,(\text{dB}) + V_{Rx}\,(\text{dB}) - 3 \tag{2}$$

$$\phi V_{IF} = \phi V_{LO} + \phi V_{Rx} \tag{3}$$

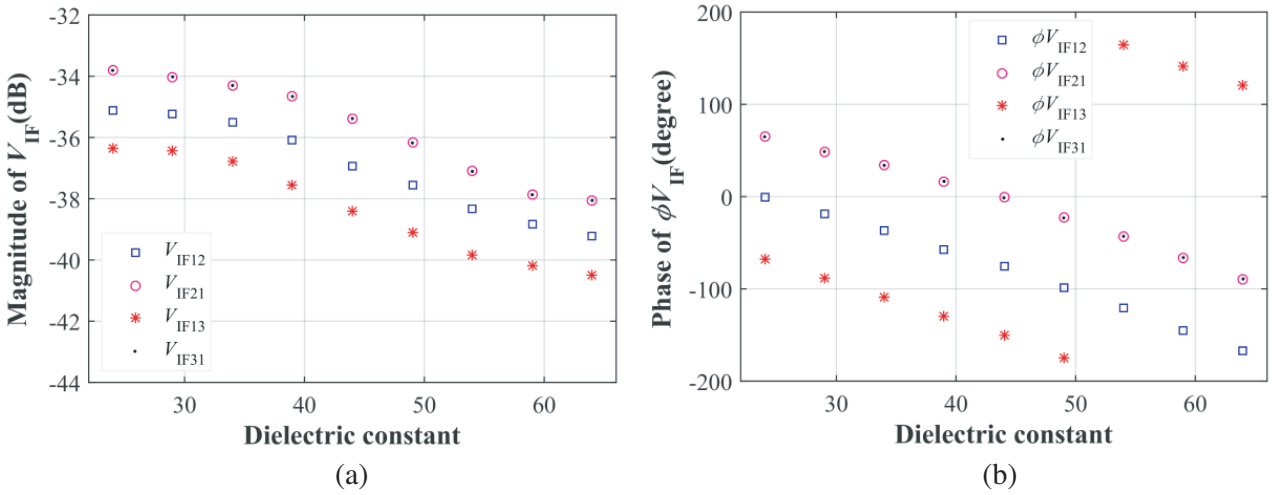

Figure 5. Simulation result of (a) magnitude and (b) phase of IF transmission through sugar solution.

thus total parameters were V_{IF12} V_{IF21} V_{IF13} V_{IF31} and ϕV_{IF12} ϕV_{IF21} ϕV_{IF13} ϕV_{IF31}. The analysis result was found when ε'_r was 24, and the magnitudes of V_{IF12} V_{IF21} V_{IF13} V_{IF31} were -35.1, -33.4, -36.4, and -33.4 dB, respectively. When ε'_r increased to 29, 34, 39, and 64, V_{IF} continuously decreased to -39.22, -38.06, -40.5 and -38.06 dB, in the same way (Fig. 5(a)). Further, considering ϕV_{IF}, when ε'_r increased from 24 to 64, all ϕV_{IF} parameters decreased from -0.57, 64.86, -67.75, and 64.86 degrees to -167.23, -89.21, 120.08, and -89.21 degrees, as shown in Fig. 5(b).

The simulation result shows that when ε'_r of sugar solution increases from 24 to 64, the power V_{IF} from mixed-signal decreases because the attenuation is directly related to the dielectric constant. At the same ε'_r, the attenuation of the transmission wave with high frequency is more than low frequency; thus, the magnitudes of V_{IF21} and V_{IF31} are equal, and the highest V_{IF12} and V_{IF13} are lower. The ϕV_{IF} increased when the ε'_r of the medium was higher; at the same ε'_r, high frequency was affected more than low frequency. Thus, these results nonetheless show the possibility of SSC classification from the V_{IF} and ϕV_{IF} of an X-band signal at a distance, as designed.

4. PROPOSED SENSOR SYSTEM

The proposed SSC of sugar solution determination sensor system used transmission triple-frequency signal in X-band, which consists of 2 pairs of frequency modules, 10.2 with 10.4 GHz and 10.2 with 10.6 GHz, each pair operating transmitting and receiving signals alternatively. The power of transmission through sugar solution of each frequency pair was mixed with LO by a mixer in the receiver to produce 2 IF outputs, for down convert frequency of received signal to operating range of a gain and phase detector (AD8302), which were then compared to determine the gain and phase difference for the use in SSC of sugar solution analysis. The proposed system consists of a module that contains a dielectric resonator oscillator (DRO), two array patch antennas, a frequency mixer for signal generation, transmission, reception, and mixing with LO, a relay for DC voltage supplying control, RF switch for data selection, gain and phase detector for IF signal comparison and microcontroller Arduino UNO for system control. The structure of the proposed system is shown in Fig. 6.

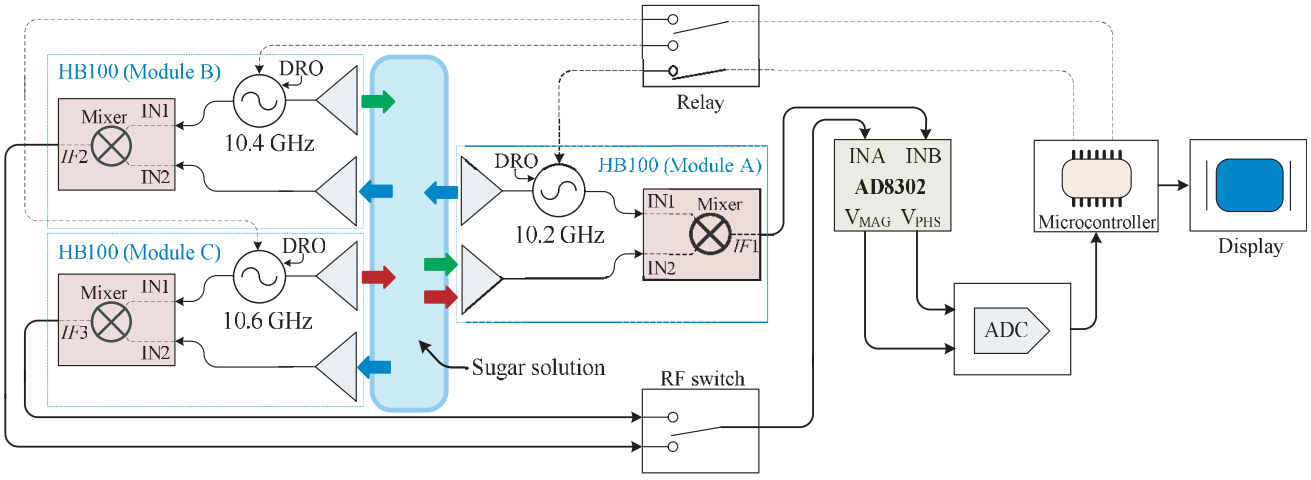

Figure 6. The schematic of the proposed sensor system.

To reduce system cost, the sensor system was designed with a low-cost transceiver module HB100. In the sensor system includes three transceiver modules HB100: module A, module B, and module C. The DROs of A, B, and C modules were tuned simply by turning the metallic screw on the DRO, generating signals at 10.2, 10.4, and 10.6 GHz, respectively. The module operates signal generation, transmission, reception, and mixing with LO, in which each pair of modules alternately operates. Modules A and B operate, then modules A and C operate, to prevent the interference between 2 frequency pairs. Transceiver modules were installed in the same position as in simulation, where module A was placed opposite modules B and C, and a sample holder with size $10 \times 20 \times 7$ cm was in the middle

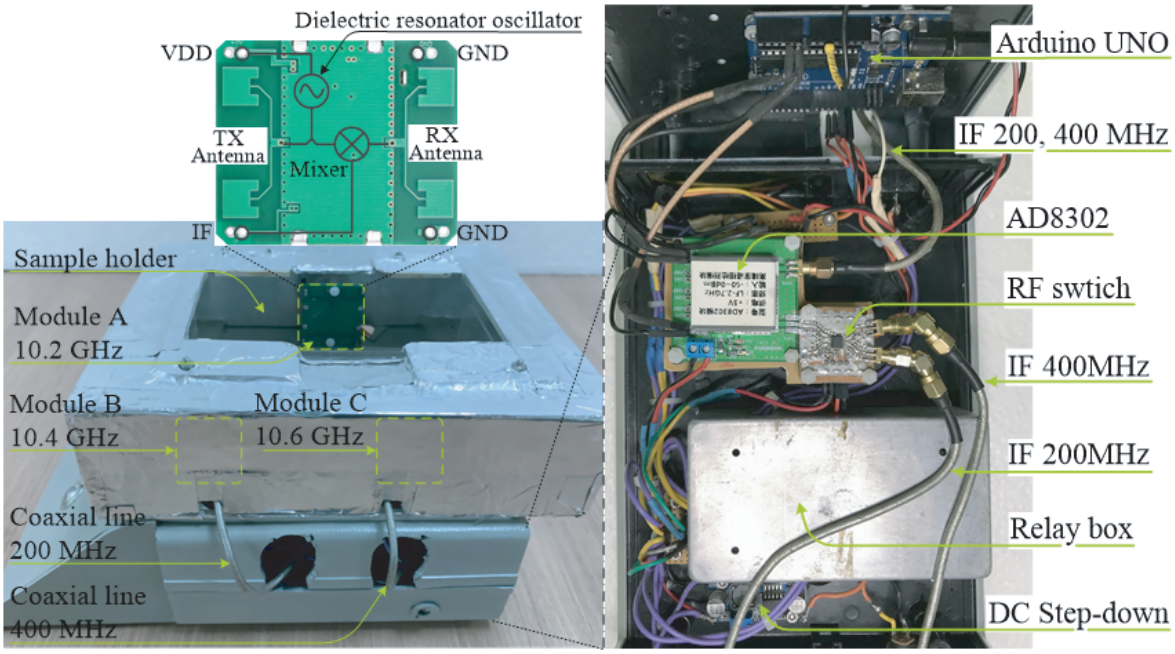

Figure 7. (a) Internal and (b) external of SSC level determination sensor system prototype.

(Fig. 7(a)). Each pair of modules was controlled to generate a signal simultaneously by DC voltage supplying control from the relay, which made the phase comparison of IF signal effective; furthermore, modules were controlled to alternately operate. The generated signal was transmitted from each module and mixed with LO at the receiver in the paired module, but the mixer output was filtered only at low frequencies. Each module pair operated in the same way, producing IF output at 200 MHz from the first pair and 400 MHz from the second pair. The 2 IF outputs from paired module were sent to AD8302 for magnitude ratio and phase difference comparison in Equations (4) and (5).

$$V_{MAG} = K_M \log(V_{INA}/V_{INB}) + 0.9 \tag{4}$$

$$V_{PHS} = K_P \left[\phi V_{INA} - \phi V_{INB} - 90^\circ\right] + 0.9 \tag{5}$$

The voltages V_{INA} and V_{INB} are input to ports INA and INB of the AD8302, respectively. K_M and K_P are constants set to 0.03 V/decade and -0.01 V/degree, respectively. The IF from module A was sent to AD8302 input A, and the RF switch switched input B to receive from module B or C. The outputs of comparison from the first pair was V_{MAG1} and V_{PHS1}, and those from the second pair were V_{MAG2} and V_{PHS2}, which were DC voltage types that were converted by 10-Bit analog to digital converter. The entire sensor system operation was controlled by Arduino UNO broad, and the internal structure of the sensor system prototype is shown in Fig. 7(b).

5. EXPERIMENTAL SETUP

5.1. Data Collection

In experiment, sugar solution was in a sample holder with a height ranging from 2 to 8 cm, and the measured results revealed a gain and phase difference of each SSC level at heights 7 and 8 cm, implying that the height of sugar solution in the experiment was 7 cm for measurement performance. The sugar solution was in the sample holder with size $3.2 \times 18.2 \times 7.2$ cm that was placed in the middle of modules then transmitted and received signal through sugar solution to measured V_{MAG1} V_{PHS1} V_{MAG2} and V_{PHS2} at 14 different SSC levels including 3, 6, 9, 13, ..., 45° Brix, where each sample was measured 5 times and calculated the average value for accuracy measurement data. The V_{MAG1} and V_{MAG2} from

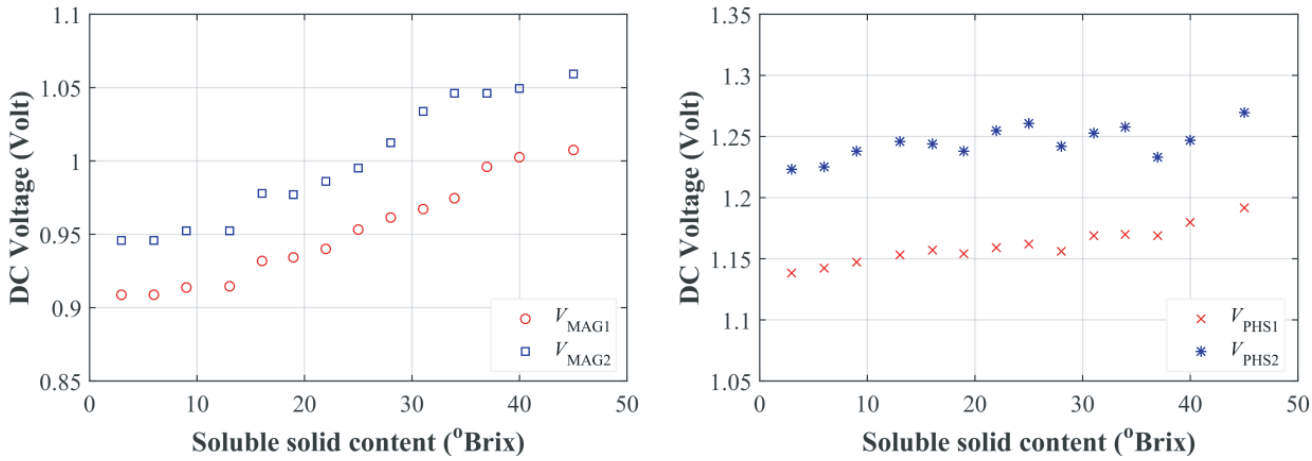

Figure 8. Relation between (a) SSC level V_{MAG} and (b) SSC level and V_{PHS}.

the lowest SSC at 3° Brix were 0.909 and 0.946; when being measured at 6° Brix, they were 0.909 and 0.946; and when SSC increased to 9° Brix, they were 0.914 and 0.952 volt, and continuously increased with an increase in SSC from 13, 16 to 45° Brix in 0.914 to 1.007 and 0.953 to 1.06 volt, respectively (Fig. 8(a)). V_{PHS1} increased slightly from 3 to 45° Brix sugar solution in the range of 1.138 to 1.19 volt, whereas V_{PHS2} slightly increased from 3 to 25° Brix sugar solution in the range of 1.223 to 1.26 volt and from 28 to 45° Brix sugar solution in the range of 1.242–1.27 volt (Fig. 8(b)).

The sensitivity of V_{MAG1}, V_{MAG2}, V_{PHS1}, and V_{PHS2} was 7.8, 9.3, 3, and 1.8 mV/3° Brix, respectively. Although the sensitivity of system was low, the system was still able to operate. The stability of the proposed determination system was confirmed by calculating the standard deviation (SD) of five voltage measurements for each sample. The lowest SDs in V_{MAG1} and V_{MAG2} were 0.0033 and 0.0061, respectively. The lowest SDs were higher in V_{PHS1} and V_{PHS2} (0.013 and 0.0164, respectively) than in V_{MAG1} and V_{MAG2} but were still acceptable. The measurement result shows that V_{MAG} responds to SSC changes because the magnitude and phase changes of the transmission signal are nonlinear. Increase of SSC makes the magnitude ratio between signal 10.2 and 10.6 GHz (V_{MAG2}) more than the ratio between 10.2 and 10.4 GHz (V_{MAG1}), and the decrease of phase between 10.2 and 10.6 GHz is (V_{PHS2}) more than that between 10.2 and 10.4 GHz (V_{PHS1}). The correlations (R^2) between SSC and V_{MAG1} and V_{MAG2} are 0.973 and 0.966, respectively, indicating that V_{MAG1} and V_{MAG2} change in the same trend, but the magnitude of V_{MAG2} has a wider range than V_{MAG1} because medium attains transmission signal power at a high frequency more than low frequency, resulting in a clearer measurement result in each SSC level. V_{PHS1} is related to $R^2 = 0.895$, and V_{PHS2} is related to SSC less than 25° Brix, but some intervals are nonlinear. Therefore, for the system to be effective in classifying the SSC levels, ANNs were used in the decision part with V_{MAG1}, V_{MAG2}, V_{PHS1}, and V_{PHS2} data for training and testing for structure optimization, input node, and SSC classification ability.

5.2. ANNS Training Method

The structure of ANNs type multilayer perceptron (MLP) consists of input i node $\mathbf{v}_1$, $\mathbf{v}_2$, ..., $\mathbf{v}_i$ weight $\mathbf{w}_{1j}$, $\mathbf{w}_{2j}$, ..., $\mathbf{w}_{ij}$, system bias $\mathbf{b}_k$, and $\mathbf{v}_k$ that was a summation of weight multiply with input and bias (Fig. 9). Then, $\mathbf{v}_k$ was used to calculate output $\mathbf{y}_k$ with nonlinear activate sigmoid function (y_{sig}) shown in Equation (6).

$$y_k = y_{sig}\left(\underbrace{\sum_{j=1}^{m} w_{ij}x_j + b_k}_{v_k}\right) \tag{6}$$

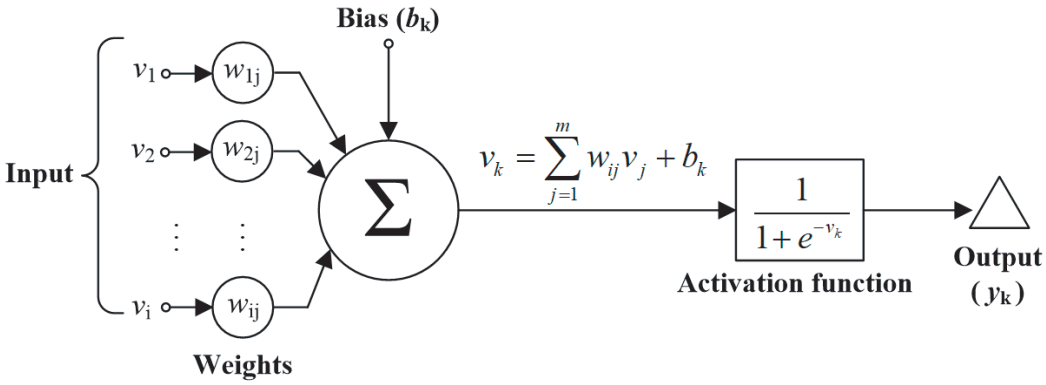

Figure 9. Structure of MLP network with one hidden layer.

ANNs training for decision-making in sensor systems used input variables to optimize weight with 4 input data V_{MAG1}, V_{MAG2}, V_{PHS1}, and V_{PHS2} from measurements of 14 SSC levels of sugar solution, and each data has 406 data points. All data points were randomly divided into 3 sets including dataset A, dataset B, and dataset C. The number of input nodes and data division for training, validation, and testing of each dataset was defined in Table 1. The target of ANNs training was SSC level of sugar solution ranging from 3, 6, 9 to 45° Brix, that map to 4 binary bits [38] for the complexity of the training process reduction, thus the number of output nodes was 4 to represent 14 SSC levels shown in Table 2.

Table 1. Training data of artificial neural networks.

Dataset	A	B	C
Data input	$V_{MAG1,2}$	$V_{MAG1,2}$ V_{PHS1}	$V_{MAG1,2}$ $V_{PHS1,2}$
Data points	406×2	406×3	406×4
Training (31%)	126×2	126×3	126×4
Validation (31%)	126×2	126×3	126×4
Test (38%)	154×2	154×3	154×4

Table 2. Relationship between SSC level and mapping function of targets.

Mapping function	0001	0010	0011	≈	1100
Targets (° Brix)	3	6	9		45

The ANNs structure for the decision part in the system consists of 3 layers: input layer, hidden layer, and output layer. The input layer received V_{MAG1}, V_{MAG2}, V_{PHS1}, and V_{PHS2} from the sensor and was varied from 2 to 4 nodes related to the number of input parameters as $\mathbf{v}_1$, $\mathbf{v}_2$ to $\mathbf{v}_i$. In the hidden layer, the number of hidden nodes, $\mathbf{h}_1$, $\mathbf{h}_2$ to $\mathbf{h}_j$, were varied from 4, 6, 8, and 10 nodes. The output layer consists of 4 nodes, $\mathbf{y}_1$, $\mathbf{y}_2$ to $\mathbf{y}_4$, and outputs from the training were compared with target $\mathbf{t}_1$, $\mathbf{t}_2$ to $\mathbf{t}_4$ to fine-tune the error used to tune $\mathbf{w}_{11}$ $\mathbf{w}_{12}$ to $\mathbf{w}_{j4}$ for error reduction. ANNs structure from training is shown in Fig. 10.

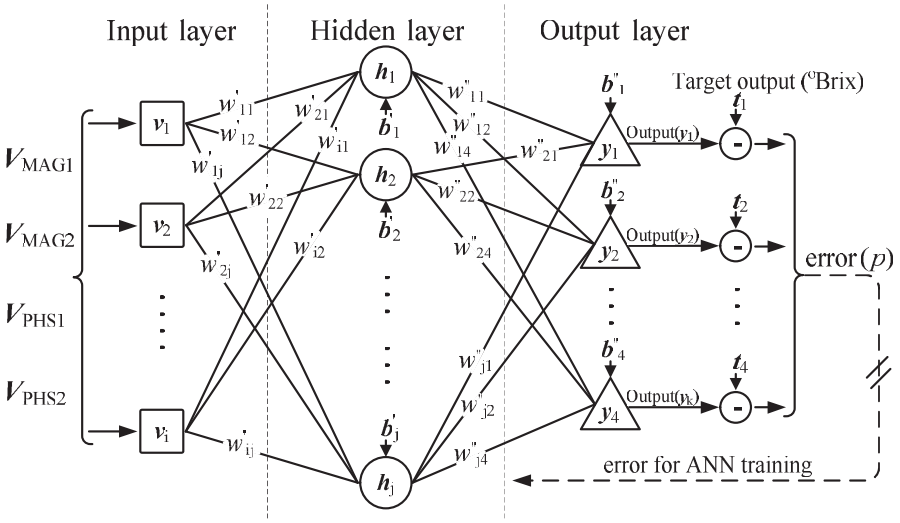

Figure 10. Proposed model of artificial neural network.

6. RESULT AND DISCUSSION

6.1. ANNS Result Analysis

To evaluate the performance of the ANNs model, input nodes, hidden nodes, and learning rates were varied. The learning rate was tested using various datasets, and the optimal value was 0.012. When the error rate was less than 10^{-3}, or the epoch exceeds 500, the neural network stops training. Training started with dataset A, and hidden nodes ranging from 4, 6, 8, and 10 nodes provided mean square error (MSE) values of 0.074, 0.055, 0.05, and 0.042 (Fig. 11(a)) because of the difficulty of learning with only 2 trained data inputs. When dataset B was used as input training, ANNs learned more efficiently; however, when 4 hidden nodes were used in training, ANNs still learned hard and had a high MSE at 0.059. When 6 hidden nodes were used, learning was more efficient, providing less MSE at 0.022, and when 8 hidden nodes were used ANNs learning continuously increased efficiency, providing MSE at 1.031×10^{-2}. Finally, after training with 10 hidden nodes, MSE was slightly reduced at epoch less than 300, indicating that the system became more complex as the number of hidden nodes increased. However, increasing the epoch makes ANNs better at learning, and the MSE at 1.14×10^{-2} (Fig. 11(b)) shows that increased input data improve ANNs' learning. When learning with dataset C, ANNs performed well except when using 4 hidden nodes because nonlinear input and number of hidden nodes were insufficient for learning, then provided MSE 0.0402. When the number of hidden nodes was increased to 6 nodes, learning fluctuated slightly at first but can learn and provide MSE at 0.0122. When the number of hidden nodes was increased to 8 and 10 nodes, MSE fluctuated slightly at epoch less than 300, but at 500 epochs, learning of 8 and 10 hidden nodes was efficient and provided MSE at 2.71×10^{-3} and 2.661×10^{-3} (Fig. 11(c)).

It can be observed from the number of input and hidden nodes of ANN optimization to find suitable weights that the number of input nodes affects the learning and solving capability of the decision system. The ANN testing result shows that training with dataset A did not provide good learning capability because it was insufficient, and the number of hidden nodes at 4 or 6 nodes cannot solve complicated problems. Considering 8 and 10 hidden nodes, testing accuracy was 66.82% and 67.14%, respectively, which is sufficient for use in the decision-making process of systems. For dataset B, using 3 input nodes when training with 4 and 6 hidden nodes, learning was more accurate but still below 70%. When the hidden node was increased to 8 and 10 nodes, MSE decreased, and accuracy increased to 78.1% and79.08%, respectively. The last input data training was dataset C since using more input data, accuracy slightly increased when the number of hidden nodes was 4 and 6 nodes, and when using 8 hidden nodes, learning was efficient and provided an accuracy of 92.98%. When using 10 hidden nodes, ANNs learning was slightly more efficient with an accuracy of 93.55%, which is approximate to 8 hidden

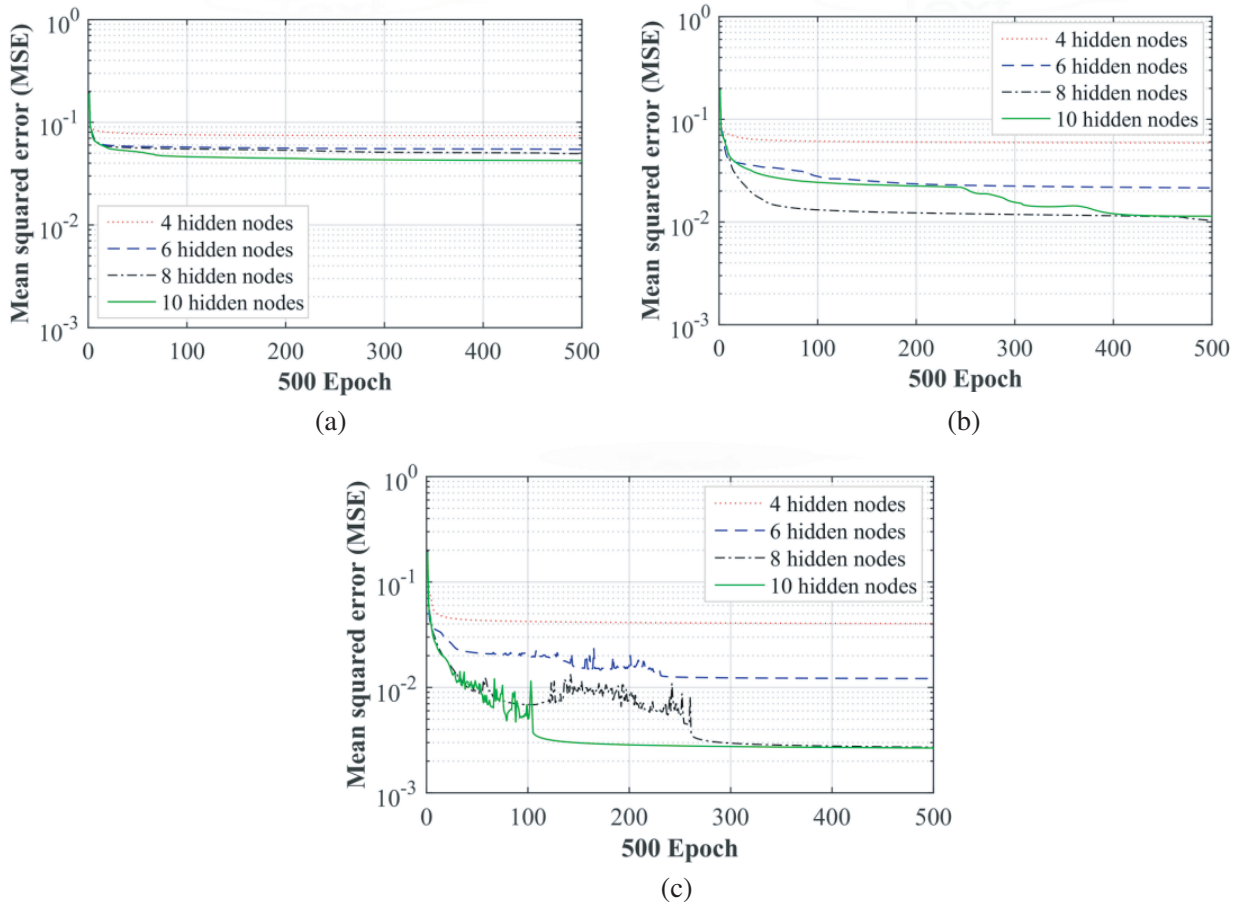

Figure 11. Performance plots of all neural networks, (a) dataset A, (b) dataset B, (c) dataset C.

Table 3. Performance of ANNs training and testing.

Input node	Hidden Node	MSE	Training performance		Validation performance		Testing performance	
			Error	Acc.	Error	Acc.	Error	Acc.
2	8	4.959e-02	4.748e-02	74.60%	5.885e-02	71.13%	0.1517	66.82%
	10	4.237e-02	4.132e-02	73.02%	5.734e-02	70.27%	0.1432	67.14%
3	8	1.031e-02	9.653e-03	94.44%	9.813e-03	88.10%	3.086e-02	78.10%
	10	1.14e-02	1.003e-02	93.65%	1.018e-02	87.84%	2.995e-02	79.08%
4	8	2.71e-03	2.641e-03	98.41%	9.261e-03	93.2%	1.211e-02	92.98%
	10	2.661e-03	2.580e-03	97.62%	8.182e-03	94.6%	1.127e-02	93.55%

nodes at the same epoch 500 (Table 3).

The result shows that training with 4 input nodes resulted in a good performance, thus dataset C, which included V_{MAG1}, V_{MAG2}, V_{PHS1}, and V_{PHS2}, was suitable for use. When the performances of SSC level classification at 8 and 10 hidden nodes were compared, the results were close. Because of the complexity and resource used, 8 hidden nodes were suitable for applications. The ANNs structure, which consists of 4 input nodes, 8 hidden nodes, and 4 output nodes, was implemented only Equation (6) on the Arduino UNO microcontroller board to serve as the decision part of the sensor system using 8,716 bytes of memory and 542 bytes of variable memory. Furthermore, Arduino UNO broad was used to control system synchronized operations, allowing SSC level determination to be done in real-time.

6.2. Testing and Evaluation of the ANNS Model

The decision performance of ANNs was tested for error analysis SSC level of sugar solution determination from 3, 6 to 45° Brix 154 samples, with 11 samples for each SSC level. The percentage error from the decision was calculated using Equation (7),

$$\%\text{Error} = \frac{N_{Test} - N_{Mea}}{N_{Test}} \times 100 \tag{7}$$

where the number of the tested samples at each SSC level is N_{Test}, and the number of right decision samples is N_{Mea}. The decision result of ANNs at each SSC level provided maximum error at 27.3% of 16° Brix because of measurement data V_{MAG1} close to V_{MAG2} of 16 and 19° Brix thus provided 2nd maximum error of 18.2% at 19° Brix. The 3rd maximum error was 9.1% at 6, 31, and 40° Brix (Fig. 12).

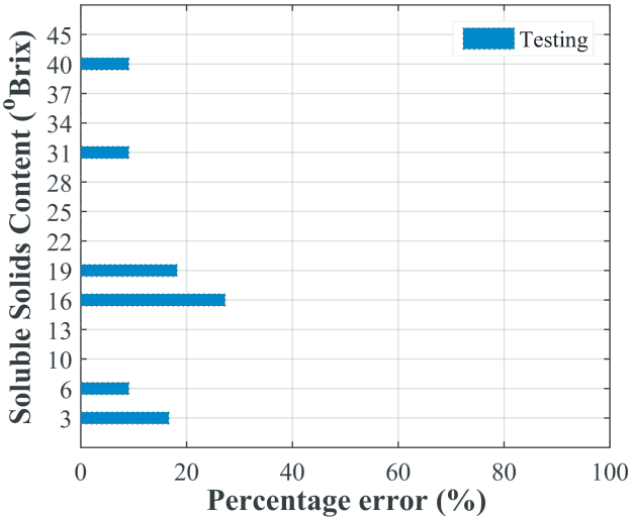

Figure 12. Percentage error of testing result.

The novelty of this work is the measurement technique that uses two pairs of frequencies mixing combining with ANNs. The advantages of this system are low cost and non-contact measurement in which the ANNs can afford low complexity and resource savings. The sensor system was easy to use by implementation in a microcontroller board. The SSC levels in solution were analyzed in a previous work; however, they are invasive measurement with sugar solution [22–24] and contact with sample holder [20, 21], in addition, parameter measurement for processing used equipment in laboratory, high cost, and skilled operator required. The sensor systems are compared with those of previous sugar-content measurement techniques in Table 4.

6.3. Discussion

In addition to ANN decision error, some errors were from sample holding in the sample holder and bubbles during sample change. Therefore, the height of sugar solution in sample holders must be at the same level in each measurement, and measured SSC during sugar solution sample should not ripple and contain no bubble before decision-making. This control was efficient to reduce the error of measurement with the transmission. The SSC sensor system based on the transmission coefficient is not suitable for a large volume sample solution because the width of the sample solution affects the attenuation of transmission. Then the received power is not enough to process, and the accuracy of the system is low. As the voltages V_{MAG1}, V_{MAG2}, V_{PHS1}, and V_{PHS2} measured in the prototype system are not appreciably different at different Brix levels, decisions based on a particular parameter may be inaccurate. Therefore, the measured voltages were averaged to improve the system accuracy. Temperature affects the change in value of ε_r. However, in normal environment, the effect of temperature

Table 4. The comparison of the real-time sugar content measurement technique characteristic.

Ref.	Sensing Technique	Analyzed parameters	Frequency (GHz)	Installation	Measurement Device	Handling
[22]	Microstrip Antenna	Reflection coefficient	3.2, 8.7, 11.6, 14.5	Invasive	VNA	Training is required
[20]	RFID	Sensitivity	0.915	Contact	RFID reader	Skilled operator is required
[23]	Dipole antenna	Reflection coefficient	1.1–3.3	Invasive	VNA	Training is required
[24]	Microstrip antenna	Reflection coefficient	3.2–10.6	Invasive	VNA	Training is required
[21]	Resonator	Transmission coefficient	1.10, 2.20	Contact	VNA	Training is required
This work	**Microstrip antenna**	**Intermediate Frequency**	**10.2, 10.4, 10.6**	**Noncontact**	**System prototype**	**Easy to use**

is not significant, and also ANN is used for data processing, thus the effect of temperature has been reduced substantially. In addition, the sensor system had controlled effect of electromagnetic wave by shielding to prevent interference from external electromagnetic wave, thus the system was more accurate. Although the Q-factor of sensor system is not so high, V_{IF} spectrum measurement from HB100 module in low frequency to 2.7 GHz can improve for less distortion in the system and no interference from other frequencies. In addition, the power below -60 dBm is out of AD8302 operating range that makes the sensor system more stable. The low SDs verified the stability of the system. Furthermore, the presented system accurately processed four measured voltages with an ANN and was implemented in a microcontroller board. The designed device is suitable for field measurement as it has low cost and displays the SSC level in real time.

7. CONCLUSION

The SSC of sugar solution determination with triple-frequency transmission in X-band started with dielectric properties measurement of sugar solution that had different 14 SSC levels ranging from 3, 6, 9 to 45° Brix, and their ε_r', and ε_r'' were in the range 61.73 to 25.22 and 31.2 to 18.66, respectively. The ε_r' from different SSC levels was used to develop a sugar solution model, which was then used to simulate a sensor system with a sugar solution model and 3 microstrip patch antennas in the same way as the system diagram and used ε_r change related to SSC level. The simulation resulted in a relationship between the magnitude and phase of the S-parameter and ° Brix. Three transceiver modules were used to create the prototype system, which included two transceiver antennas, a frequency mixer circuit, and a DRO. Each module was tuned to operate at 10.2, 10.4, and 10.6 GHz. The module was programmed to work in pairs, 10.2 with 10.4 GHz and 10.2 with 10.4 GHz, and the transmission signals of each paired were mixed to generate IF signals with frequencies 200 and 400 MHz. The 2 IF signals of each paired module were compared to calculate the magnitude ratio and phase difference using gain and phase detector (AD8302), which provided an output as a DC voltage. The 14 SSC levels solution samples were measured as V_{MAG1}, V_{MAG2}, V_{PHS1}, and V_{PHS2}, with results ranging from 0.748 to 0.847, 0.786 to 0.899, 1.223 to 1.277, and 1.123 to 1.192 volts, respectively. All measurement data points were randomly divided into three sets as datasets A, B, and C. The optimized dataset for ANNs training was dataset C, which has four input nodes and eight hidden nodes that use worth memory to store weight and reduce processor complexity. Four output nodes were mapped to binary bits that represented the SSC level and learning rate of 0.012. The MSE was 2.71×10^{-3}, and the testing accuracy was 92.98%, demonstrating that a low-cost X-band sensor can classify SSC level determination in real-time.

REFERENCES

1. Witek, K., K. Wydra, and M. Filip, "A high-sugar diet consumption, metabolism and health impacts with a focus on the development of substance use disorder: A narrative review," *Nutrients*, Vol. 14, 1–23, 2022.
2. WHO, "Diabetes," Apr. 2021, http://www.who.int/news-room/fact-sheets/detail/diabetes.
3. Saeedi, P., I. Petersohn, P. Salpea, B. Malanda, S. Karuranga, N. Unwin, S. Colagiuri, L. Guariguata, A. A. Motala, K. Ogurtsova, J. E. Shaw, D. Bright, and R. Williams, "Global and regional diabetes prevalence estimates for 2019 and projections for 2030 and 2045: Results from the International Diabetes Federation Diabetes Atlas, 9th edition," *Diabetes Research and Clinical Practice*, Vol. 157, 1–10, 2019.
4. Erickson, J., B. Sadeghirad, L. Lytvyn, J. Slavin, and B. C. Johnston, "The scientific basis of guideline recommendations on sugar intake," *Annals of Internal Medicine*, Vol. 166, No. 4, 256–267, Feb. 2017.
5. Kumari, P. K., S. Akhila, Y S. Rao, and B. R. Devi, "Alternative to artificial preservatives," *Systematic Reviews in Pharmacy*, Vol. 10, No. 1, 99–102, 2019.
6. Allcott, H., B. B. Lockwood, and D. Taubinsky, "Should we tax sugar-sweetened beverages? an overview of theory and evidence," *Journal of Economic Perspectives*, Vol. 33, No. 3, 202–227, 2019.
7. Pelle, F. D., A. Scroccarello, S. Scarano, and D. Compagnone, "Silver nanoparticles-based plasmonic assay for the determination of sugar content in food matrices," *Analytica Chimica Acta*, Vol. 1051, No. 21, 129–137, Mar. 2019.
8. Donga, H., K. Xiaoa, Y. Xianb, and Y. Wub, "Authenticity determination of honeys with non-extractable proteins by means of elemental analyzer (EA) and liquid chromatography (LC) coupled to isotope ratio mass spectroscopy (IRMS)," *Food Chemistry*, Vol. 240, 717–724, Feb. 2018.
9. Jaywant, S. A., H. Singh, and K. M. Arif, "Sensors and instruments for brix measurement: A review," *Sensors*, Vol. 22, 1–20, 2022.
10. Menezes, N. M. C., D. A. Longhi, B. O. Ortiz, A. F. Junior, and G. M. F. de Aragão, "Modeling the inactivation of *Aspergillus fischeri* and *Paecilomycesniveus* ascospores in apple juice by different ultraviolet light irradiances," *International Journal of Food Microbiology*, Vol. 333, Nov. 2020.
11. Balogun, M. A., O. A. Abiodun, F. L. Kolawole, R. M. O. Kayode, and O. E. Olushola, "Physicochemical and sensory properties of blends of pineapple-carrot wine," *Journal of Microbiology Biotechnology Food Sciences*, Vol. 7, No. 3, 306–311, 2017.
12. Joshi, V. K., R. Sharma, V. Kumar, and D. Joshi, "Optimization of a process for preparation of base wine for cider vinegar production," *Proceedings of the National Academy of Sciences, India Section B: Biological Sciences*, 1007–1016, 2019.
13. Zaukuu, J. Z., J. Sóos, Z. Bodor, J. Felföldi, I. Magyar, and Z. Kovacs, "Authentication of Tokaj wine (Hungaricum) with the electronic tongue and near infrared spectroscopy," *Journal of Food Science*, Vol. 84, No. 12, 3437–3444, 2019.
14. Bahrami, M. E., M. Honarvar, K. Ansari, and B. Jamshidi, "Measurement of quality parameters of sugar beet juices using near-infrared spectroscopy and chemometrics," *Journal of Food Engineering*, Vol. 271, 1–7, 2020.
15. Kamboj, U., N. Kaushal, and S. Jabeen, "Near infrared spectroscopy as an efficient tool for the qualitative and quantitative determination of sugar adulteration inmilk," *Journal of Physics: Conference Series*, Vol. 1531, No. 012024, 1–8, Oct. 2020.
16. Thanavanich, C., N. Phuangsaijai, C. Thiraphatchotiphum, P. Theanjumpol, and S. Kittiwachana, "Instant quantification of sugars in milk tablets using near-infrared spectroscopy and chemometric tools," *Scientific Reports*, Vol. 12, 1–9, 2022.
17. Belay, A. and G. Assefa, "Concentration, wavelength and temperature dependent refractive index of sugar solutions and methods of determination contents of sugar in soft drink beverages using laser lights," *Journal of Lasers, Optics & Photonics*, Vol. 5, No. 2, 1–5, Jul. 2018.

18. Tao, Y., B. Yan, N. Zhang, M. Wang, J. Zhao, H. Zhang, W. Chen, and D. Fan, "Microwave vacuum evaporation as a potential technology to concentrate sugar solutions: A study based on dielectric spectroscopy," *Journal of Food Engineering*, Vol. 294, 110414, 2021.
19. Thomason, S. J. and K. S. Bialkowski, "Dielectric spectroscopy based determination of sugar content in Solution," *IEEE Sensor Letter*, Vol. 3, No. 5, 1–4, May 2019.
20. Ennasar, M. A., O. E. Mrabet, K. Mohamed, and M. Essaaidi, "Design and characterization of a broadband flexible polyimide RFID tag sensor for NaCl and sugar detection," *Progress In Electromagnetics Research C*, Vol. 94, 273–283, 2019.
21. Hosseini, N. and M. Baghelani, "Selective real-time non-contact multi-variable water-alcohol-sugar concentration analysis during fermentation process using microwave split-ring resonator based sensor," *Sensors and Actuators A*, Vol. 325, No. 112695, 1–10, Jul. 2021.
22. Islam, M. T., Md. N. Rahman, M. S. J. Singh, and Md. Samsuzzaman, "Detection of salt and sugar contents in water on the basis of dielectric properties using microstrip antenna-based Sensor," *IEEE Access*, Vol. 6, 4118–4126, Jan. 2018.
23. Rajendran, J., S. K. Menon, and M. Donelli, "A novel liquid adulteration sensor based on a self complementary antenna," *Progress In Electromagnetics Research C*, Vol. 103, 97–110, 2020.
24. Logeswaran, J. and R. B. Rani, "UWB antenna as a sensor for the analysis of dissolved particles and water quality," *Progress In Electromagnetics Research Letters*, Vol. 106, 31–39, 2022.
25. Banerjee, A., A. Kumar, N. K. Tiwari, and M. J. Akhtar, "Design of slotted microwave sensor for evaluation of water quality," *2022 IEEE Microwaves, Antennas, and Propagation Conference (MAPCON)*, 331–335, Bengaluru, India, 2022.
26. Zhao, C., G. Wu, and Y. Li, "Measurement of water content of oil-water two-phase flows using dual frequency microwave method in combination with deep neural network," *Measurement*, Vol. 131, 92–99, Jan. 2019.
27. Kazemi, N., M. Abdolrazzaghi, P. Musilek, and M. Daneshmand, "A temperature-compensated high-resolution microwave sensor using artificial neural network," *IEEE Microwave and Wireless Components Letters*, Vol. 30, No. 9, 1531–1309, 2020.
28. Zhang, J., D. Du, Y. Bao, J. Wang, and Z. Wei, "Development of multifrequency-swept microwave sensing system for moisture measurement of sweet corn with deep neural network," *IEEE Transactions on Instrumentation and Measurement*, Vol. 69, No. 9, 6446–6454, Sep. 2020.
29. Leekul, P., P. Wongsiritorn, and P. Chaisaeng, "Development of humidity monitoring system in greenhouse with electromagnetic X Band and artificial neural networks," *Progress In Electromagnetics Research M*, Vol. 100, 93–103, 2021.
30. Sumranbumrung, R., P. Khunkitti, A. Siritaratiwat, and A. Kruesubthaworn, "Characterization model of dielectric properties of cane sugar solution over 0.5–14 GHz," *IEEE Transactions on Instrumentation and Measurement*, Vol. 70, 1–8, May 2021.
31. Shiraga, K., T. Suzuki, N. Kondo, T. Tajima, M. Nakamura, H. Togo, A. Hirata, K. Ajito, and Y. Ogawa, "Broadband dielectric spectroscopy of glucose aqueous solution: Analysis of the hydration state and the hydrogen bond network," *The Journal of Chemical Physics*, Vol. 142, No. 234504, 1–13, 2015.
32. Turgul, V. and I. Kale, "Permittivity extraction of glucose solutions through artificial neural networks non-invasive microwave glucose sensing," *Sensors and Actuators A*, Vol. 277, 65–72, 2018.
33. Leekul, P., B. Mgawe, T. Kazema, H. N. Dao, P. Sirisuk, and M. Krairiksh, "Dielectric constant determination using dual doppler modules," *2021 IEEE Conference on Antenna Measurements & Applications (CAMA)*, 269–270, 2021.
34. Leekul, P., B. Mgawe, T. Kazema, H. N. Dao, P. Sirisuk, and M. Krairiksh, "Simple and effective design concept for constructing In-Situ soil dielectric property sensor with dual low-cost COTS microwave modules," *IEEE Access*, Vol. 10, 54516–54524, 2022.
35. Mishra, M., A. Rajput, P. K. Gupta, and B. Mukherjee, "Low profile, wideband, high gain CDRA with microstrip Feed for ISM and C band applications," *Progress In Electromagnetics Research C*, Vol. 126, 77–90, 2022.

36. Nguyen, V. T. and C. W. Jung, "Impact of dielectric constant on embedded antenna efficiency," *International Journal of Antennas and Propagation*, Vol. 758139, 1–6, 2014.
37. Pozar, D. M., *Microwave Engineering*, John Wiley & Sons, Hoboken, NJ, 2012.
38. Leekul, P., T. Limpiti, and P. Chaisaeng, "An intelligent humidity control system for mushroom growing house by using beam-switching antennas with artificial neural networks," *International Journal of Electrical and Computer Engineering (IJECE)*, Vol. 13, No. 1, 549–560, 2023.